JOURNAL OF PETROLOGY | VOLUME 49 | NUMBER 4 | PAGES 823–839 | 2008 | doi:10.1093/petrology/egm033

Olivine in the Udachnaya-East Kimberlite (Yakutia, Russia): Types, Compositions and Origins

VADIM S. KAMENETSKY[1,2]*, MAYA B. KAMENETSKY[1,2], ALEXANDER V. SOBOLEV[2,3], ALEXANDER V. GOLOVIN[4], SYLVIE DEMOUCHY[5], KEVIN FAURE[6], VICTOR V. SHARYGIN[4] AND DMITRY V. KUZMIN[2,4]

[1]ARC CENTRE OF EXCELLENCE IN ORE DEPOSITS AND SCHOOL OF EARTH SCIENCES, UNIVERSITY OF TASMANIA, HOBART, TAS. 7001, AUSTRALIA

[2]MAX PLANCK INSTITUTE FOR CHEMISTRY, GEOCHEMISTRY DIVISION, MAINZ, 55020, GERMANY

[3]VERNADSKY INSTITUTE OF GEOCHEMISTRY, RUSSIAN ACADEMY OF SCIENCES, MOSCOW 119991, RUSSIA

[4]INSTITUTE OF GEOLOGY AND MINERALOGY SB RAS, NOVOSIBIRSK 630090, RUSSIA

[5]DEPARTMENT OF GEOLOGY AND GEOPHYSICS, UNIVERSITY OF MINNESOTA, MINNEAPOLIS, MN 55455, USA

[6]NATIONAL ISOTOPE CENTRE, GNS SCIENCE, PO BOX 31-312, LOWER HUTT, NEW ZEALAND

RECEIVED JANUARY 22, 2007; ACCEPTED JUNE 13, 2007
ADVANCE ACCESS PUBLICATION 28 JULY 2007

Olivine is the principal mineral of kimberlite magmas, and is the main contributor to the ultramafic composition of kimberlite rocks. Olivine is partly or completely altered in common kimberlites, and thus unavailable for studies of the origin and evolution of kimberlite magmas. The masking effects of alteration, common in kimberlites worldwide, are overcome in this study of the exceptionally fresh diamondiferous kimberlites of the Udachnaya-East pipe from the Daldyn–Alakit province, Yakutia, northern Siberia. These serpentine-free kimberlites contain large amounts of olivine (~50 vol.%) in a chloride–carbonate groundmass. Olivine is represented by two populations (olivine-I and groundmass olivine-II) differing in morphology, colour and grain size, and trapped mineral and melt inclusions. The large fragmental olivine-I is compositionally variable in terms of major ($Fo_{85–94}$) and trace element concentrations, including H_2O content (10–136 ppm). Multiple sources of olivine-I, such as convecting and lithospheric mantle, are suggested. The groundmass olivine-II is recognized by smaller grain sizes and perfect crystallographic shapes that indicate crystallization during magma ascent and emplacement. However, a simple crystallization history for olivine-II is complicated by complex zoning in terms of Fo values and trace element contents. The cores of olivine-II are compositionally similar to olivine-I, which suggests a genetic link between these two types of olivine. Olivine-I and olivine-II have oxygen isotope values (+5·6 ± 0·1‰ VSMOW, 1 SD) that are indistinguishable from one another, but higher than values (+5·18 ± 0·28‰) in 'typical' mantle olivine. These elevated values probably reflect equilibrium with the Udachnaya carbonate melt at low temperatures and ^{18}O-enriched mantle source. The volumetrically significant rims of olivine-II have constant Fo values (89·0 ± 0·2 mol%), but variable trace element compositions. The uniform Fo compositions of the rims imply an absence of fractionation of the melt's Fe^{2+}/Mg, which is possible in the carbonatite melt–olivine system. The kimberlite melt is argued to have originated in the mantle as a chloride–carbonate liquid, devoid of 'ultramafic' or 'basaltic' aluminosilicate components, but became olivine-laden and olivine-saturated by scavenging olivine crystals from the pathway rocks and dissolving them en route *to the surface. During emplacement the kimberlite magma changed progressively towards an original alkali-rich chloride–carbonate melt by extensively crystallizing groundmass olivine and gravitational separation of solids in the pipe.*

KEY WORDS: *kimberlite; olivine; partial melting; carbonatitic melt; oxygen isotopes; H_2O*

*Corresponding author. Telephone: 61-3-62267649. Fax: +61-3-62262547. E-mail: dima.kamenetsky@utas.edu.au

INTRODUCTION

Kimberlites are rare and compositionally unusual among terrestrial magmas, but their intimate relationships with diamonds make them invaluable to the scientific and exploration communities. The association of kimberlites with diamonds and deep-seated mantle xenoliths links the origin of parental kimberlite magmas to the greatest known depths (>150 km) of magma derivation (e.g. Dawson, 1980; Pasteris, 1984; Mitchell, 1986, 1995; Eggler, 1989; Girnis & Ryabchikov, 2005). At the same time, kimberlite magmas are amongst the least viscous and most buoyant of all magmas, which allows exceptionally rapid transport from the source region (Eggler, 1989; Canil & Fedortchouk, 1999; Haggerty, 1999; Kelley & Wartho, 2000; Sparks *et al.*, 2006) and preservation of diamonds. The physical properties of a kimberlite magma relate to the enrichment in carbonate components, which are represented in common kimberlites by calcite and dolomite. The abundant carbonate component in kimberlite rocks is counterbalanced by a more abundant olivine (ultramafic) component, represented by olivine fragments and crystals that are commonly affected by serpentinization.

Kimberlites are characteristically enriched in highly incompatible elements, with extreme fractionation between lithophile elements of contrasting incompatibility, and a genetic link to the parental melts of carbonatites and olivine melilitites is thus possible (Brey & Green, 1976). The work by David H. Green and his colleagues has provided invaluable insights into the compositions of low-degree mantle melts and the role of alkali and volatile elements in the processes of mantle melting and metasomatism (Green & Wallace, 1988; Wallace & Green, 1988; Falloon & Green, 1989, 1990; Green, 1990; Green *et al.*, 1990; Sweeney *et al.*, 1995). One of the most significant achievements of the experimental school of David Green was a demonstration of primary sodic dolomitic carbonatite at the solidus of a carbonated garnet-lherzolite (Green & Wallace, 1988; Wallace & Green, 1988; Falloon & Green, 1990). Mantle-derived alkali carbonate melts were further considered as an important metasomatizing agent in the mantle and lithosphere (Brenan & Watson, 1991; Yaxley *et al.*, 1991, 1998; Dalton & Wood, 1993*a*).

Such an alkali (>3–5 wt% Na_2O) carbonate melt, poor in SiO_2 (~3–6 wt%) and H_2O (~1–2 wt%) (Wallace & Green, 1988; Falloon & Green, 1990; Brenan & Watson, 1991; Yaxley & Green, 1996), must play an important role in the genesis of kimberlite primary magmas. However, kimberlites worldwide demonstrate low alkali abundances, especially Na_2O (<0·3 wt%), and very high H_2O (>4–5 wt%). The apparent conflict between experimental results and data on natural kimberlite magmas can be resolved if kimberlites from the Udachnaya-East pipe (Daldyn–Alakit province, Siberian craton, Fig. 1) are considered to be representative of a kimberlite magma prior to alteration (Marshintsev, 1986; Kamenetsky *et al.*, 2004, 2007*a*, 2007*b*; Maas *et al.*, 2005). The Udachnaya-East kimberlites sampled from deep horizons (>400 m) show no signs of alteration (i.e. chlorite and serpentine are absent), which is reflected in low H_2O contents (<0·5 wt%) and enrichment in alkalis (3·5–6·2 wt% Na_2O; 1·6–2·2 wt% K_2O). Importantly, all other key petrographic and compositional features of the unaltered Udachnaya-East kimberlites remain undistinguishable from those of Group-I kimberlites worldwide [see comparison given by Kamenetsky *et al.* (2007b)].

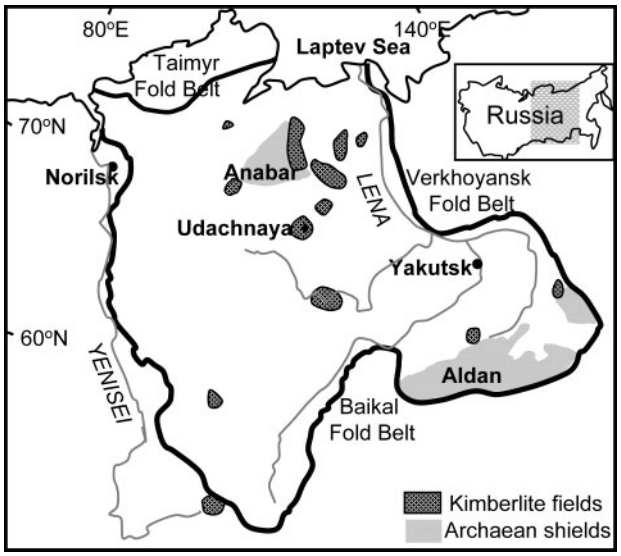

Fig. 1. Map of the Siberian Platform showing the major kimberlite fields after Pearson *et al.* (1995).

Kimberlites worldwide are rich in olivine, both entrained by and crystallized from the melt (Mitchell, 1973, 1986; Moore, 1988; Arndt *et al.*, 2006). Thus, the obvious mismatch between kimberlites and experimental melts at the peridotite solidus (Wallace & Green, 1988; Falloon & Green, 1990) is the significant depletion, and possibly even undersaturation (Sweeney *et al.*, 1995), of the carbonatitic melt in the olivine component. Unfortunately, the masking effects of alteration, common in kimberlites, do not permit routine recognition of olivine generations, and so the olivine component originally dissolved in the kimberlite parental melt remains controversial. The unaltered Udachnaya-East kimberlites provide an unique opportunity for recognition of olivine populations and olivine paragenetic assemblages. The results of this study suggest a complex interplay between mantle-derived alkali carbonate melt and olivine-rich upper mantle and lithosphere that ultimately produces the magmas and rocks known as kimberlites.

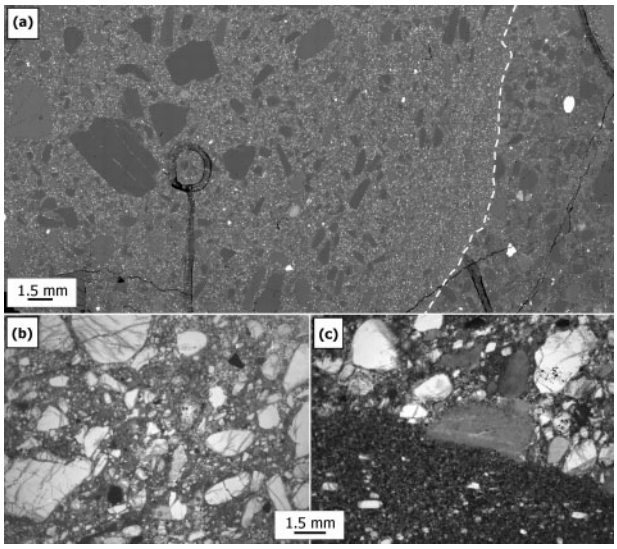

Fig. 2. Back-scattered electron image (a) and photomicrographs in plane-polarized light (b, c) showing the main petrographic features of unaltered kimberlites. Distinct contacts between typical porphyroclastic textures and rare aphanitic textures are demonstrated in (a) and (c). Olivine-I is represented by fragments and round crystals. Olivine phenocrysts are set in a carbonate–chloride–olivine groundmass. (See Fig. 6 for more details of kimberlite textures and morphological features of olivine.)

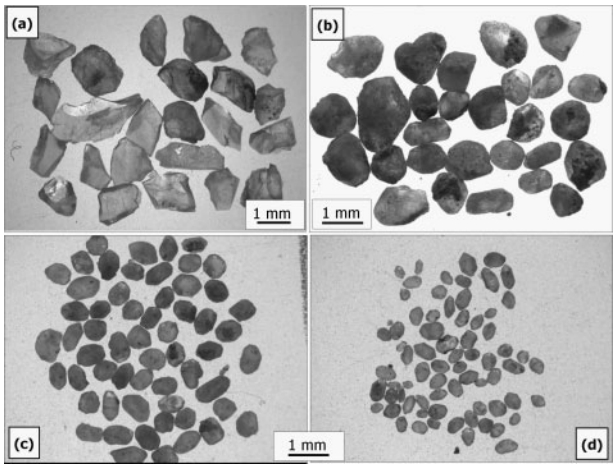

Fig. 3. Two populations of olivine: clear angular grains of olivine-I (a), round to euhedral crystals of 'transitional' population, fraction size 0·5–1 mm (b); 0·3–0·5 mm (c) and <0·1–0·3 mm (d) fractions of euhedral unambiguously groundmass olivine-II.

SAMPLES AND METHODS

Udachnaya-East kimberlite

The ~350 Ma Udachnaya pipe, the best known example of twin diatremes, is located in the NW part of the Daldyn field of the Siberian diamondiferous province (Fig. 1). It consists of two adjacent bodies (East and West) that become separated at 250–270 m depth. The pipe has a complex structure, which reflects multiple events of magma injection. The samples studied belong to the latest stages of emplacement of the multiphase Udachnaya-East pipe (Marshintsev, 1986; Zinchuk *et al.*, 1993). The rocks are characterized by the petrographic features, mineralogy, chemical and isotopic compositions (Marshintsev *et al.*, 1976; Marshintsev, 1986; Sobolev *et al.*, 1989; Golovin *et al.*, 2003; Kamenetsky *et al.*, 2004, 2007*a*; Maas *et al.*, 2005) of most common Type-I (Mitchell, 1989) or Group-I (Smith, 1983) kimberlites.

The Udachnaya-East kimberlites are olivine-rich rocks (Fig. 2), a feature shared by the majority of known kimberlites, excluding rare aphanitic kimberlites, such as those from Kimberley, South Africa (Shee, 1986; Edgar *et al.*, 1988; Edgar & Charbonneau, 1993; le Roex *et al.*, 2003) and Jericho, Canada (Price *et al.*, 2000). Aphanitic varieties among the Udachnaya-East kimberlites are also present on a small scale, either showing sharp linear contacts with, or grading into the more common porphyritic rocks (Fig. 2a and c). The large abundance of olivine in our samples (45–60 vol.%) is reflected in the high MgO content in the bulk-rock compositions (28–35 wt%). Olivine is set in a fine-grained matrix of carbonates [calcite, shortite $Na_2Ca_2(CO_3)_3$ and zemkorite $(Na, K)_2Ca(CO_3)_2$], chlorides (halite and sylvite), and minor phlogopite and opaque minerals [e.g. spinel group minerals, perovskite, Fe ± (Ni, Cu, K) sulphides].

Sample preparation

Olivine was released from the kimberlite by gentle crushing to 1–2 mm size and subsequent dissolution of matrix carbonates and chlorides in 10% HCl. Then olivine was sorted by size and euhedral crystals were hand-picked from fragmentary grains (Fig. 3). Several thousand euhedral crystals (size fraction 0·3–0·5 mm) from three porphyritic samples were mounted in epoxy, and ground to approximately the mid-plane surfaces for further analytical studies. Such a method is advantageous compared with traditional studies of polished sections because it applies to a much larger population of grains from a larger rock sample, distinguishes between crystal populations based on their size and shape, provides 3D observation of grain interiors, and allows precise control of grain positioning, sectioning and exposure of olivine-hosted inclusions. Conventional studies of polished sections were also carried out.

Measurement of major and trace elements in olivine

Quantitative element analysis and mapping of olivine were performed using a JEOL Superprobe JXA-8200 electron microprobe (Max Planck Institute for Chemistry, Mainz, Germany). The analytical conditions were 20 kV accelerating voltage and 20 nA primary electron beam current,

with 60 s peak and 30 s background counting times (Sobolev *et al.*, 2007). Back-scattered electron imaging (BSE) and element mapping were used to examine the 2D distribution of elements across grain surfaces. Measurements were done in the stage scanning mode, registering simultaneously X-ray signals of five wavelength-dispersive spectrometers and a BSE image. Step intervals were 1–2 μm and X-ray acquisition time per step was 100–300 ms. Measurements were interpreted using the built-in JEOL Map Analysis Software.

Morphology, zoning and textural relationships of olivine were studied in three samples by BSE imaging of the entire surface of polished sections. Mapping was performed using a FEI Qanta 600 scanning electron microscope and EDAX energy-dispersive X-ray analysis system (CSL, University of Tasmania). A series of individual BSE images were collected (40 nA emission current, 25 kV accelerating voltage, 1024 × 800 pixels frame resolution), and then joined together using the Mineral Liberation Analyser (MLA) software (written at the Julius Kruttschnitt Mineral Research Centre, University of Queensland).

Measurement of H_2O in olivine

Fourier-transform IR spectroscopy (FTIR) was used for analysis of H_2O in doubly polished olivine crystals (~500 μm thick). The analyses were performed at the University of Minnesota using a FTIR Nicolet Magna-IR 750 spectrometer coupled with an IR microscope and equipped with a KBr beam splitter and a MCT (mercury–cadmium-telluride) detector. A square aperture $100 \times 100\ \mu m^2$ was chosen for the analyses and 200 scans were accumulated to obtain the absorbance spectra. A series of spectra were collected at a spacing of 50 μm across the olivine samples along the longest axis to check for the homogeneity of the hydroxyl distribution. Despite some parts of the olivine being cloudy or milky, the analysed spots and paths across each of the olivine crystal were in all cases free of cracks or inclusions, and were clean and transparent (no turbid, cloudy or milky areas). The water content (i.e. hydrogen detected as a hydroxyl bond determined from the stretching frequencies) and the homogeneity of the hydroxyl distribution within our samples were analysed using unpolarized IR radiation.

After background-baseline correction and thickness normalization to 1 cm, the hydroxyl content was determined for each spectrum using the calibration given by Paterson (1982). This calibration, which may underestimate the water content for some minerals (Libowitzky & Rossman, 1996; Bell *et al.*, 2003), is based on an empirical correlation between OH stretching frequency and extinction coefficient:

$$C_{OH} = \frac{\varphi_i}{150\xi} \int \frac{k(\nu)}{3780 - \nu} d\nu$$

where C_{OH} is the concentration of hydroxyl as a function of φ_i, ξ is an orientation factor that equals 1/3 for unpolarized measurements, and $k(\nu)$ is the absorption coefficient for a given wavenumber ν. φ_i is a density factor, whose value is chemistry dependent; $\varphi_i = 4{\cdot}39 \times 10^4 H/10^6 Si$ or 2695 ppm H_2O wt% for olivine Fo_{90}. Integration was performed from $\nu = 3200$ to $3600\ cm^{-1}$.

Measurement of oxygen isotopes in olivine

Fractions of euhedral crystals and fragments of olivine from four samples were analysed separately for their oxygen isotope composition at the National Isotope Centre, GNS Science (New Zealand). Olivine grains were pretreated with BrF_5 overnight to remove any surface or water contamination. After evacuation in a sample chamber oxygen was extracted by heating the samples with a CO_2-laser in a BrF_5 atmosphere, similar to the method described by Sharp (1990). The evolved O_2 was converted to CO_2 and analysed on a Europa GEO 20-20 mass spectrometer. Oxygen yields from olivine varied between 96 and 102%. Values are reported in the familiar $\delta^{18}O$ notation, relative to VSMOW. Samples were normalized to the international quartz standard NBS-28 (NIST SRM 8546) using a value of +9·6‰. Values for six NBS-28 standards analysed with the samples varied by less than 0·1‰ from each other.

OLIVINE MORPHOLOGY AND COMPOSITION

Two populations of olivine in the Udachnaya-East kimberlite can be recognized based on size, colour, morphology, and entrapped inclusions (Figs 2–4 and 6). Consistent with many other studies of kimberlitic olivine (e.g. Mitchell, 1973, 1978; Emeleus & Andrews, 1975; Barashkov & Mahotko, 1977; Boyd & Clement, 1977; Hunter & Taylor, 1984; Sobolev *et al.*, 1989; Nielsen & Jensen, 2005), the populations are represented by olivine-I (interpreted by different workers as cognate phenocrysts or xenocrysts) and groundmass olivine-II. However, as indicated by descriptions and discussion below, the two populations overlap significantly in terms of their composition, and possibly origin.

Olivine-I

Light green or light yellow olivine-I is present as rounded and oval crystals, or more often as angular fragments with smooth edges (Figs 3a, b and 4a, b). Angular olivine-I is characteristically transparent and large (0·5 to 7–8 mm, Figs 3a and 4a, b), whereas ovoid grains are smaller (0·7–2 mm) and often 'dusted' with inclusions (Fig. 3b). It should be noted that olivine grains in Fig. 3b cannot be confidently assigned to either population. Melt and fluid inclusions occur only in 'secondary' trails along healed

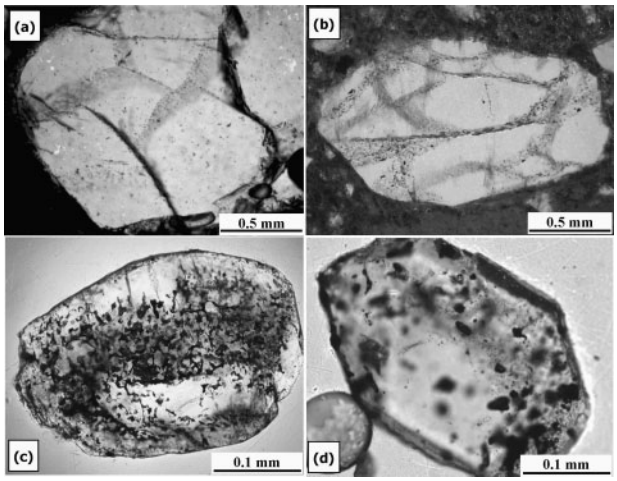

Fig. 4. Photomicrographs in plane-polarized light of individual crystals of olivine-I (a, b) and olivine-II (c, d) showing networks of magmatic inclusions, including carbonate–chloride melt inclusions. Details of melt inclusions in the studied samples have been given in several earlier publications (Golovin *et al.*, 2003, 2007; Kamenetsky *et al.*, 2004, 2007*a*).

fractures in angular olivine-I and some round crystals (Fig. 4a and b).

Olivine-I is characterized by variable forsterite content (Fo) from 85 to 94 mol%, although most grains are Fo >91 (Fig. 5a and Supplementary Data, available for downloading at http://www.petrology.oxfordjournals.¥org/). Most grains appear to be homogeneous, at least in terms of their Fo content, except the outermost rims and around healed fractures. Abundances of minor elements Ca, Ni, Cr and Mn in olivine-I vary strongly with Fo content (Fig. 5a). Compositional trends resembling fractionation can be seen for NiO (decreasing from 0·43 to 0·13 wt%) and MnO (increasing from 0·07 to 0·17 wt%) as the Fo content decreases (Fig. 5a). However, it should be noted that NiO in the majority of olivine-I is almost constant (0·35–0·39 wt%). CaO increases in $Fo_{94–90}$ (0–0·05 wt%) and remains constant as olivine-I becomes less forsteritic (Fig. 5a).

Unpolarized FTIR spectra of the nine largest (>0·8 mm) euhedral olivine crystals from the aphanitic zone of sample K24/04 are typical of kimberlite-derived olivine (Matsyuk & Langer, 2004) with the main IR bands located at 3572 and 3525 cm^{-1}. Additional IR bands at wavenumbers >3600 cm^{-1} could be due to hydrous mineral impurities such as humite and serpentine (Miller *et al.*, 1987; Matsyuk & Langer, 2004). The corresponding water contents, after application of the calibration of Paterson (1982), range from 10 to 136 ppm H_2O (Table 1). Three crystals have surprisingly low water contents (10–36 ppm) and have IR characteristics similar to those of olivine from peridotite xenoliths in alkali basalts (e.g. Demouchy *et al.*, 2006; Peslier & Luhr, 2006). A FTIR profile across the olivine crystal ol-2 demonstrated homogeneous distribution of hydroxyl bands.

Olivine-II: morphology and zoning

Olivine-II is represented by relatively small (0·05–0·8 mm), euhedral, flattened grains (Figs 3c, d and 4c, d). Crystals display a tabular habit (tablet shape), and crystal growth is preferentially developed in the {100} and {001} directions. Olivine-II is colourless or slightly greenish or brownish; the presence of a large amount of various inclusions is responsible for the weak transparency and 'cloudy' appearance of their host crystals (Figs 3c, d and 4c, d).

Morphology and zoning of olivine can be observed in polished sections (Fig. 6); however, for the purpose of the statistical study we examined several thousands of individually picked and epoxy-mounted olivine grains and recorded 296 BSE images of individual olivine-II crystals in a single grain-mount. Olivine-II demonstrates compositional variability (Table 2 and Supplementary Data) in terms of its Fe–Mg relationships (higher and lower Fo correspond to darker and lighter areas, respectively; Figs 6 and 7). Nearly all the groundmass olivine crystals, even the smallest, exhibit intra-grain compositional variability (Figs 6, 7 and 8). The commonly used term 'zoning' is not quite appropriate in the case of the Udachnaya-East olivine-II, as is evident from the description below. Several main types of olivine compositional 'structure' account for most typical Fo variations within single grains (Fig. 7):

(1) a single core, euhedral, subhedral, or round in shape, that can be more forsteritic (~70%; Figs 6, 7a, c, f, g and 8b) or less forsteritic (~30%; Figs 6, 7b, h, i and 8c–e) than the rim;
(2) two or more cores of different shape and composition (Fig. 7l–q);
(3) no distinct core—the grains are either compositionally uniform or have a mosaic-like structure (Fig. 7d and e).

Some cores exhibit linear features (e.g. cracks) along which the olivine composition changes (Fig. 9a). All olivine-II show abrupt change to extremely Mg-rich (Fo_{96}) compositions at the very edge of the grains (~5–10 μm thick) in contact with matrix carbonate (Fig. 8).

The grains with a single core are the most abundant (~85–90%); however, euhedral cores are very rare (5%) compared with round shapes. Some cores have almost perfect olivine crystal shapes, and as a rule the crystallographic outlines of the inner cores are parallel to the whole grain outlines (Fig. 7a, b, g and h). The majority of olivine grains have corroded core edges (Fig. 7c and d), and the degree of irregularity varies even within a single core. In other words, some outlines of the core can be straight and parallel to the crystal's outer rims, whereas

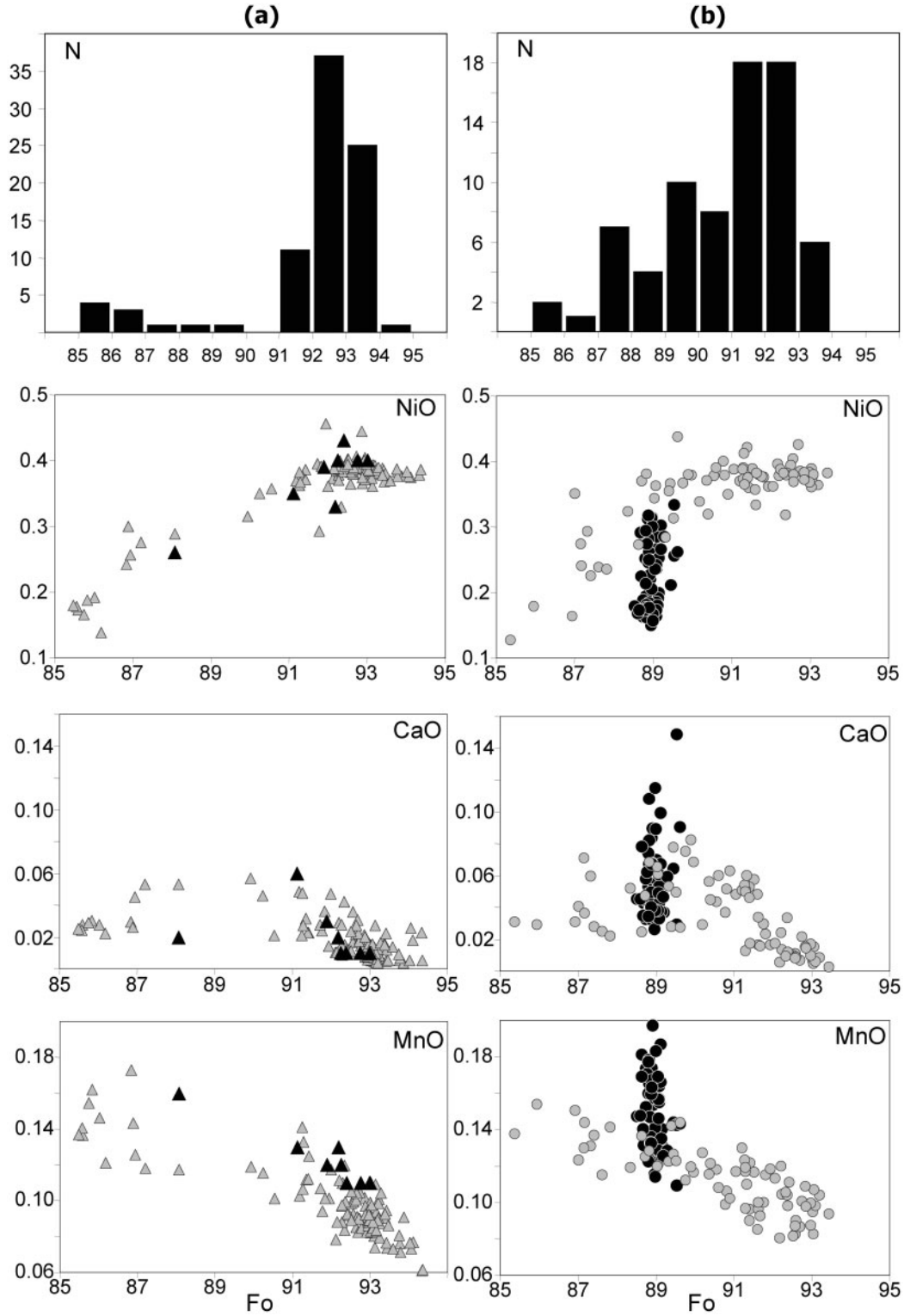

Fig. 5. Forsterite (in mol%) and trace element (in wt%) compositions of olivine-I (a) and olivine-II, 0·3–0·5 mm size (b). Olivine-I analysed for H_2O (Table 1) is shown by black triangles; grey and black circles represent cores and rims of olivine-II, respectively. N, number of grains. The analytical error (1σ, equals 0·08% for Fo, 2% for Ni, and 6% for CaO and MnO) is smaller than the size of the symbols.

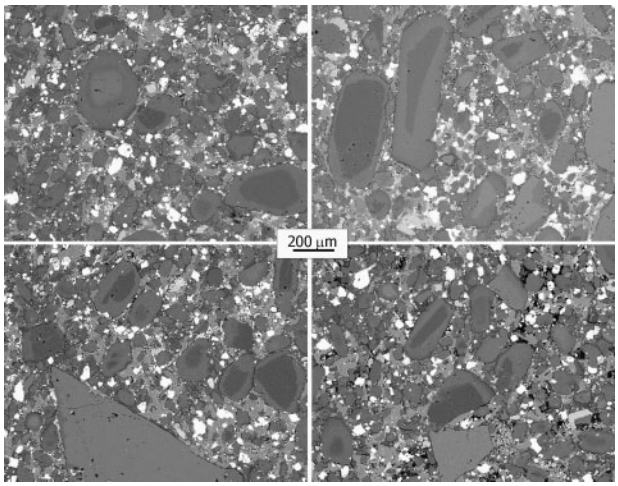

Fig. 6. Back-scattered electron images of representative areas in the hypabyssal kimberlite sample K24/04 showing the shape, size and 'zoning' patterns of olivine grains. The matrix is composed of different carbonates, chlorides and oxides.

Table 1: Major element composition (wt%) and water abundances (ppm by weight) of individual olivine-I grains from sample K24/04 (Fig. 2a)

	ol-2	ol-3	ol-4	ol-5	ol-6	ol-8	ol-9	ol-10
SiO_2	40·27	40·53	40·18	39·82	39·69	40·56	40·86	40·83
FeO	8·69	6·88	7·92	7·54	11·52	7·12	7·70	7·48
MnO	0·13	0·11	0·12	0·12	0·16	0·11	0·13	0·11
MgO	50·00	51·33	50·35	50·38	47·73	51·19	50·91	51·04
CaO	0·06	0·01	0·03	0·01	0·02	0·01	0·02	0·01
NiO	0·35	0·40	0·39	0·40	0·26	0·40	0·33	0·43
Cr_2O_3	0·05	0·04	0·02	0·03	0·02	0·05	0·04	0·03
Total	99·55	99·29	99·02	98·30	99·39	99·43	99·99	99·93
Fo (mol%)	91·12	93·01	91·89	92·25	88·07	92·76	92·18	92·40
H_2O (ppmw)	114	118	10	117	136	30	112	36

Table 2: Representative analyses of groundmass olivine II (cores and rims)

	SiO_2	FeO	MnO	MgO	CaO	NiO	Cr_2O_3	Total	Fo
core	39·80	14·09	0·14	46·14	0·03	0·13	0·00	100·33	85·4
rim	40·48	10·87	0·18	48·47	0·08	0·18	0·03	100·29	88·8
core	39·76	13·48	0·15	46·29	0·03	0·18	0·01	99·90	86·0
rim	40·37	10·87	0·16	48·46	0·05	0·19	0·04	100·14	88·8
core	39·97	12·53	0·12	47·07	0·04	0·35	0·01	100·09	87·0
rim	40·00	10·70	0·17	48·11	0·07	0·18	0·03	99·26	88·9
core	40·31	10·99	0·14	48·07	0·02	0·27	0·01	99·81	88·6
rim	40·58	10·58	0·16	48·40	0·06	0·16	0·03	99·97	89·1
core	40·30	10·60	0·12	48·31	0·07	0·34	0·04	99·78	89·0
rim	40·15	10·78	0·18	48·01	0·07	0·21	0·04	99·44	88·8
core	40·53	9·72	0·12	48·96	0·07	0·38	0·06	99·84	90·0
rim	40·34	10·61	0·16	48·55	0·06	0·17	0·06	99·95	89·1
core	40·58	8·73	0·12	49·94	0·05	0·39	0·06	99·87	91·1
rim	40·28	11·00	0·18	48·18	0·08	0·17	0·11	100·00	88·7
core	40·88	7·28	0·08	50·56	0·01	0·39	0·02	99·22	92·5
rim	40·54	10·70	0·14	48·24	0·04	0·22	0·04	99·92	88·9
core	41·14	6·93	0·10	51·47	0·01	0·37	0·01	100·03	93·0
rim	40·44	10·71	0·18	48·59	0·09	0·17	0·01	100·19	89·0
core	40·79	6·45	0·09	51·59	0·00	0·38	0·03	99·33	93·5
rim	39·83	10·77	0·17	48·11	0·07	0·18	0·05	99·18	88·8

other boundaries of the same core appear highly diffuse (Fig. 7a, f, g and j).

In the majority of zoned crystals the cores are separated from rims by a thin layer of distinct composition (Figs 7f–q and 8a, c, e; see also Fedortchouk & Canil, 2004, fig. 3). These layers are variable in shape, continuity and width. Even within a single grain the 'separating' layer shows significant variability in shape, width and composition. The composition of such layers in those grains with reverse 'zoning' is always more Fo-rich than the composition of both cores and rims (Fig. 7h, i and m–q). In the grains with normal 'zoning', the 'separating' layer can be more or less forsteritic than cores and rims.

The areas of 'cores' and 'rims' calculated from a large number of BSE images occupy in total 56 and 44%, respectively, but volumetrically the 'rims' are more dominant (~60 vol.%).

Crystals with two or three cores are relatively rare (14%), but can be very important for genetic interpretations. Typically, multi-core grains are an intergrowth of two distinct crystals, where the cores with different or similar Fo have a shape and orientation similar to those of the grain's edges (Fig. 7l–q). In grains with two or more cores of different compositions, the cores are usually separated from each other (Fig. 7l–o), although a few examples are noted where the cores coalesce (Fig. 7p and q).

Olivine-II: compositional variation

The inner parts ('cores') of olivine-II are highly variable in Fo content (85·5–93·5 mol%), although the compositions Fo 90·5–93 are most common (69%, Fig. 5b, Table 2 and Supplementary Data). The cores display a relatively wide range of NiO (0·13–0·44 wt%), CaO (0–0·08 wt%), MnO (0–0·15 wt%), and Cr_2O_3 (0–0·09 wt%) contents (Fig. 5b). NiO contents are the highest and almost constant at Fo >89·5, and then gradually decrease in less magnesian olivine. MnO contents tend to increase with decreasing Fo.

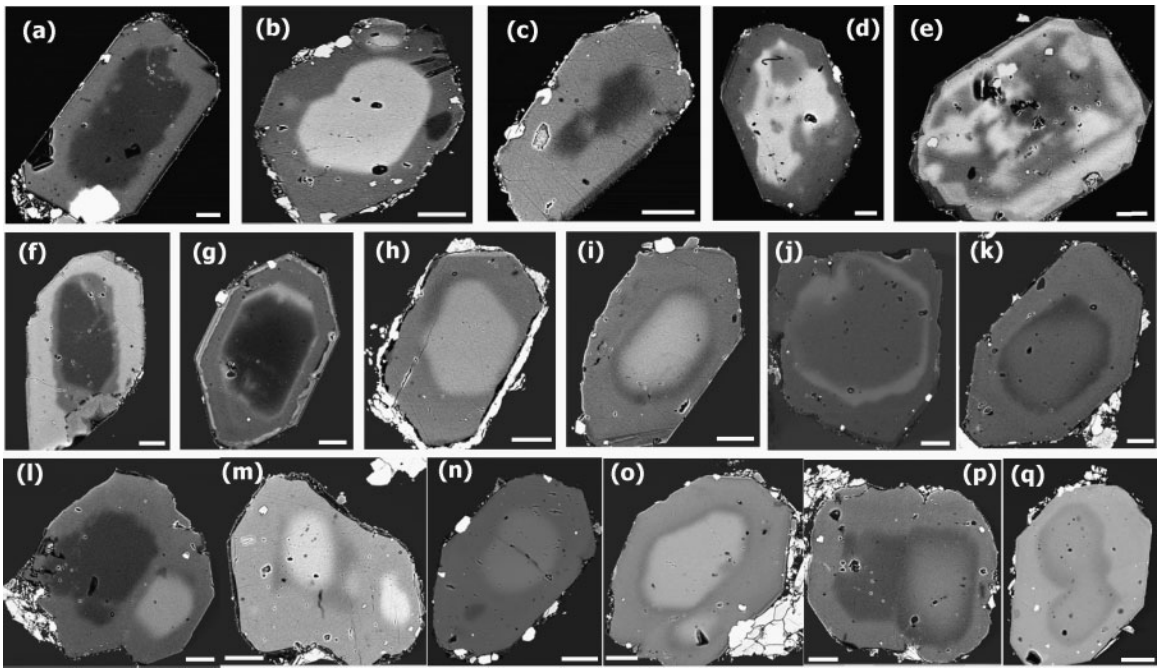

Fig. 7. Back-scattered electron images of olivine-II crystals demonstrating different types of zoning and core and rim relationships (see text for details). Scale bars represent 50 μm.

CaO abundances seem to increase (from 0 to 0·1 wt%) as Fo decreases to 89·5 mol%.

The outer parts ('rims') of olivine-II, although representing significant volumes of this population, have very constant Fo content of 89·0 ± 0·2 mol% (Fig. 5b). In contrast, the trace element abundances in the rims are highly variable (in wt%: NiO 0·15–0·35, CaO 0·03–0·15, MnO 0·11–0·2, Cr_2O_3 0·01–0·11 and Al_2O_3 0–0·04). In general, the rims are richer in MnO, but poorer in NiO than cores with the same Fo content (Fig. 5b). The outermost forsteritic (Fo_{96}) rims are very enriched in CaO (up to 1 wt%).

X-ray element maps for Fe, Ni, Ca, Al, and Cr were acquired for 55 olivine-II grains mounted individually in epoxy and exposed at the mid-plane parallel to the *c*-axis (e.g. Fig. 8). In general, the distribution of elements and their relationships are very complex, but consideration of the distribution of Fo and Ni has permitted three main groups of compositional patterns to be identified.

Compositional Pattern 1, found in 23 grains, is characterized by coupled behaviour of Fe (Fo) and Ni contents in the olivine cores. In other words, a core, defined as having distinct Fe, is clearly visible on the Ni maps (Fig. 8a–c), and in a given grain the higher Ni content corresponds to lower Fe.

Compositional Pattern 2, found in 19 grains, still shows a 'negative' correlation between Fe and Ni in the cores, but a distinct (in terms of Fe) core cannot be confidently recognized on the Ni maps (Fig. 8d).

Compositional Pattern 3, found in 13 grains, is different from the above two types in that the distribution of Ni bears no resemblance to that of Fe (Fig. 8e). For example, the cores of different shape and size, well defined on Fe maps (e.g. Fig. 8e), are not apparent based on Ni concentrations. On the other hand, the distribution of Ni throughout a significant part of these grains (excluding outmost rims and their closest 'neighbourhood') is very homogeneous and defines shapes similar to the grains' outlines. In other grains a seemingly homogeneous distribution of Fe is in contrast to the distribution of Ni and Ca, showing good crystallographic contours, largely parallel to the grain's outlines.

Unlike Fe (1/Fo), in most cases the patterns of Ni distribution demonstrate good crystallographic shapes, similar to the outer edges of the olivine grain, regardless of the number, shape and composition of the cores (in terms of Fo) present (Fig. 8). This shape always includes the core [as defined by Fe (1/Fo)], and may have the highest Ni abundances in a thin outline (Fig. 8a). Such a Ni-enriched layer has variable thickness, and its outer contour is always rectilinear, whereas the inner contour can be curved. In all grains with two or more cores, Ni defines a single zone combining all cores (Fig. 8e).

Distribution of Ca within olivine-II, despite its very low abundances, can be also useful in recognizing a transition from cores to rims (Fig. 8c and e). In all mapped grains Ca increases abruptly in very thin outer rims and along secondary fractures filled with mineral, fluid and

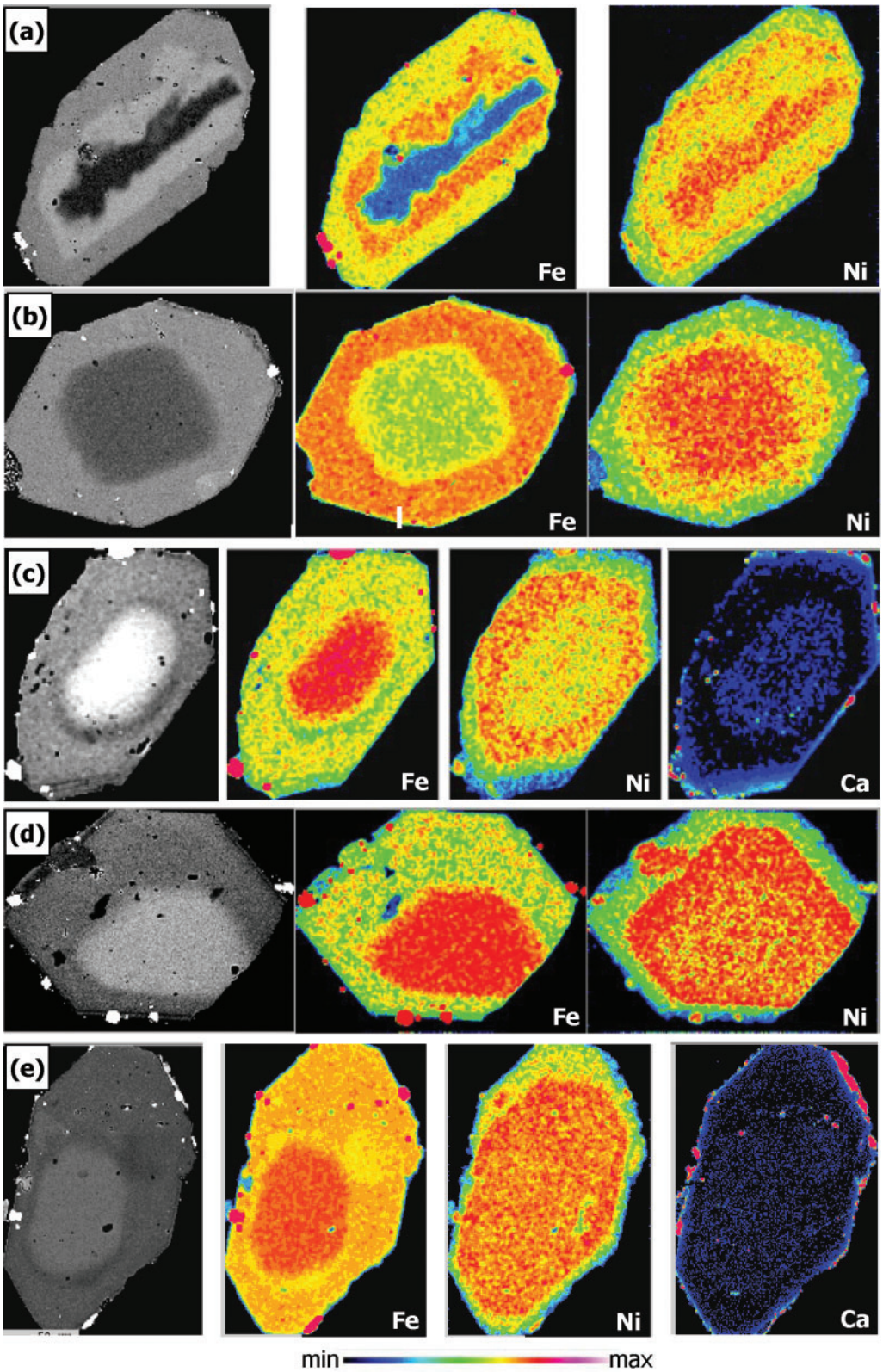

Fig. 8. Back-scattered electron images and X-ray element maps of olivine-II crystals demonstrating different types of Fo (Fe), Ni and Ca distribution (a–e). Colour scale indicates increasing intensity (and thus concentration).

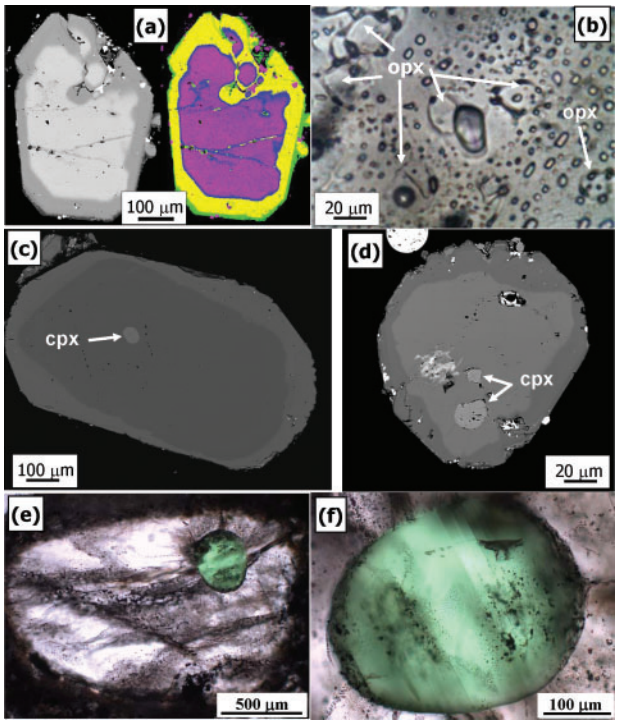

Fig. 9. Back-scattered electron images (a, c, d) and photomicrographs in plane-transmitted light (b, e, f) of mineral, fluid and melt inclusions in olivine. (a) Framework of fractures in the core of olivine-II healed with more forsteritic olivine and carbonate–chloride melt inclusions (for details see Golovin *et al.*, 2003, 2007; Kamenetsky *et al.*, 2004, 2007*a*); shown on BSE and X-ray (Fe Kα) map; (b) a cluster of coexisting orthopyroxene crystals and low-density CO_2-rich bubbles in the rim of olivine-II; (c, d) high-Ca pyroxene inclusions in high-Fo and low-Fo cores, respectively, of olivine-II; (e, f) high-Ca pyroxene inclusion in round olivine-I.

melt inclusions. The inner parts of most analysed grains show no significant gradient in Ca content (at given analytical conditions and detection limits), but in several grains (Fig. 8c and e) Ca is relatively enriched in the core parts (and 'transitional' layer, where present). Importantly, such Ca enrichment is recorded for cores and transitional layers with variable Fo contents. This is most pronounced in the grains with two cores of both different (Fig. 8e) and similar Fo values. At the same time, Ca content is minimal in those parts of olivine grains that have a Ni-enriched layer (Fig. 8c).

Oxygen isotope composition

We present for the first time $\delta^{18}O$ values of unaltered olivine from kimberlites. Both populations of the Udachnaya-East olivine crystals from four samples show similar, and restricted, oxygen isotopic values (+5·5 to +5·7‰, Table 3). These are more positive than values from unaltered mantle peridotite xenoliths (5·18 ± 0·28‰, 2 SD; Mattey *et al.*, 1994), but are similar to values obtained for olivine from oceanic arc lavas (Eiler *et al.*, 2000) and peridotite xenoliths in New Mexico alkali basalts (Perkins *et al.*, 2006). We interpret deviation from the accepted isotope values of mantle olivine by low-temperature (<700–800°C; Kamenetsky *et al.*, 2004) re-equilibration of olivine with the carbonate-rich melt of the Udachnaya kimberlite (12–14‰, Kamenetsky *et al.*, 2007*a*). Furthermore, the elevated $\delta^{18}O$ values for the Udachnaya-East kimberlite melts imply a mantle source that has an ^{18}O enrichment compared with 'typical' mantle.

Table 3: Oxygen isotope values of olivine from two populations

	$\delta^{18}O$‰ VSMOW	
	olivine-I	olivine-II
YBK-0	5·6	5·5
YBK-1	5·7	5·6
YBK-2	5·7	5·6
YBK-3	5·5	5·6

MINERAL AND MELT INCLUSIONS IN OLIVINE

Inclusions of different composition are present in almost all grains of the Udachnaya-East olivine. They can be very abundant in some grains, but rare in others. Three main types of magmatic inclusions are recognized in the studied samples: crystals, fluid and melt (see also Sobolev *et al.*, 1989). Inclusion sizes are variable (<1 to ~400 μm) and the distribution of inclusions within a single olivine crystal is very heterogeneous, with some parts totally devoid of inclusions, and some parts so packed with inclusions as to make olivine almost opaque (Figs 4 and 9e). The highest density of inclusions is observed along internal fractures and growth planes (Figs 4 and 9). Crystal inclusions in olivine of both populations are always primary. Inclusions of melt and fluid in olivine-I and cores of olivine-II are always restricted to fractures healed with olivine of different composition (Fig. 9a), and thus are secondary in origin with respect to their host olivine. Similar inclusions in the rims of olivine-II show features reminiscent of both primary and secondary origin. Melt inclusions in olivine of both populations are predominantly alkali carbonate–chloride in composition with daughter crystals of phlogopite–tetraferriphlogopite, djerfisherite, magnetite, olivine, humite–clinohumite, monticellite, rare sulphates and phosphates, and CO_2-rich bubbles (Golovin *et al.*, 2003, 2007; Kamenetsky *et al.*, 2004; Sharygin *et al.*, 2007). Silicate melt inclusions have not been found in this or other studies.

The rims of olivine-II grains contain abundant inclusions of different minerals that are never present in the cores. Among them, Cr-spinel, phlogopite, perovskite and rutile are relatively abundant, whereas magnetite and picroilmenite are less common. Inclusions of low-Ca pyroxene (Mg-number 88–92) occur in both cores and rims ($Fo_{86–91}$) in clusters of several (10–30) round and euhedral grains. A common association of low-Ca pyroxene in the rims includes numerous melt and fluid inclusions, and CO_2-rich bubbles adhering to the surfaces of the pyroxene crystals (Fig. 9b). The compositions of low-Ca pyroxene inclusions are characterized by high SiO_2 (53·3–58 wt%) and Na_2O (0·1–0·9 wt%), elevated TiO_2 (0–0·5 wt%), and low Al_2O_3 (0·7–1·4 wt%), CaO (0·7–1·7 wt%) and Cr_2O_3 (0·1–0·6 wt%), compared with mantle orthopyroxene.

Rare inclusions of high-Ca pyroxene in the Udachnaya-East olivine (Fig. 9c–f) are restricted to olivine-I and cores of olivine-II. They occur as single crystals or clusters of several crystals. They vary in size (25–400 μm), colour (emerald green to greyish green) and shape (round to euhedral–subhedral). Most of them are intimately associated with the carbonate–chloride material, which forms a coating on surfaces and inclusions inside clinopyroxene grains (Fig. 9f). The clinopyroxene inclusions (Mg-number 87·5–94·5 mol%) are in Mg–Fe equilibrium with the host olivine $Fo_{86·3–93}$, and are characterized by low Al_2O_3 (0·65–2·9 wt%), and high CaO (19·5–23·8 wt%), Na_2O (0·75–2·3 wt%) and Cr_2O_3 (0·9–2·6 wt%) contents. Individual crystals show fine-scale compositional zoning, with a general pattern of MgO and CaO increase, and Na_2O, Cr_2O_3 and, in some cases, Al_2O_3 decrease towards the rims. Major and trace element compositions of high-Ca pyroxene inclusions overlap with compositions of clinopyroxene from lherzolite nodules in the Udachnaya-East kimberlite (Fig. 10).

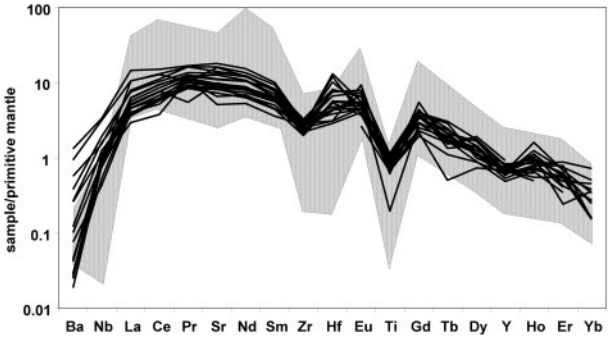

Fig. 10. Primitive mantle normalized (Sun & McDonough, 1989) compositions of high-Ca pyroxene inclusions in the cores of olivine-II (lines) in comparison with the compositions of clinopyroxene from lherzolite xenoliths in the Udachnaya-East pipe (field). Details of the samples and the analyses will be published elsewhere.

DISCUSSION

How unique is fresh olivine in kimberlites?

Olivine, although the most abundant mineral in kimberlites and that responsible for their ultramafic compositions, remains largely 'neglected' in petrological studies, and 'surprising little work has been done on the olivine' (Arndt *et al.*, 2006). The lack of free access to kimberlites, and existing restrictions on release of information to the general public because of the exceptional commercial value of kimberlites has the result that 'kimberlites are regarded by . . . the geological and geochemical community within an aura of glamour and mystique' (Eggler, 1989). Moreover, even within the 'kimberlite community' the confidentiality related to the kimberlite research limits the exchange of information about specific features of particular kimberlites. If kimberlites are to be finally 'freed from their aura of mystique' as D. H. Eggler suggested, their studies need to be more transparent.

Apart from the Udachnaya-East kimberlite, only a few examples of 'extremely fresh' and 'remarkably well-preserved' kimberlites [e.g. from Lac de Gras, Northwest Territories (Fedortchouk & Canil, 2004), West Greenland (Nielsen & Jensen, 2005; Arndt *et al.*, 2006) and the Upper Canada Gold Mine, Ontario (Watkinson & Chao, 1973)] have been reported in the literature. Although the availability of chemical analyses of groundmass olivine in the kimberlite literature is poor, the nature of the olivine zoning and compositions has either been plotted or discussed (e.g. Mitchell, 1973, 1978, 1986; Emeleus & Andrews, 1975; Reid *et al.*, 1975; Boyd & Clement, 1977; Hunter & Taylor, 1984; Moore, 1988; Skinner, 1989; Dawson, 1994; Fedortchouk & Canil, 2004; Nielsen & Jensen, 2005; Arndt *et al.*, 2006). Importantly, the olivine of the Udachnaya-East kimberlite shares the same morphological, structural and compositional features with the olivines from kimberlites worldwide.

Two populations of olivine in kimberlites: fellow-travellers or close relatives?

This work on the uniquely unaltered Udachnaya-East kimberlite concurs with what has been shown in other mineralogical studies of other kimberlites, namely, the presence of morphologically distinct populations of olivine. One population is represented by large rounded grains [olivine-I of disputed origin; 'the olivine macrocryst problem . . . remains one of the more controversial aspects of kimberlite petrology' according to Mitchell (1986)], whereas another type of olivine is typically smaller but forms better-shaped crystals (olivine-II or groundmass phenocrysts). It has been advocated in the literature that olivine may provide valuable clues to the processes of kimberlite formation, transport and emplacement (e.g. Mitchell, 1973, 1986; Barashkov & Mahotko, 1977; Boyd & Clement, 1977; Moore, 1988; Skinner, 1989; Arndt *et al.*, 2006).

Mitchell (1973, 1986) considered olivine from both populations to be phenocrysts (cognate phenocrysts of olivine-I from high-pressure crystallization of the kimberlite melt, and groundmass olivine-II), although up to 40% of olivine was assigned to a xenocrystic origin from various mantle and lithospheric sources. The xenogenic origin of all or part of olivine-I is supported by their variable and relatively low water contents (Table 1), which may reflect sampling of lithological heterogeneities in the convecting upper mantle and lithosphere by the kimberlitic magma. A similar conclusion can be endorsed by the extreme diversity of peridotite xenoliths within the Udachnaya-East kimberlite (Sobolev, 1977; Shimizu *et al.*, 1997). The absence of primary melt inclusions and the presence of Cr-diopside inclusions in olivine-I also argue against their phenocrystic origin. On the other hand, the Fo–NiO covariations in olivine-I can be typical of magmatic crystallization (Sobolev *et al.*, 2007).

A xenocrystic origin of some or all grains of olivine-I does not preclude this olivine type being overgrown by the 'phenocrystic' olivine. Both types of olivine are transported together, and thus all changes related to chemical and mechanical resorption should be equally imposed on them, making a morphological distinction subjective. Both olivine populations in the studied Udachnaya-East samples demonstrate striking compositional similarity in their Fo contents (Fig. 5) and oxygen isotope ratios (Table 3). Trace element abundances are also indistinguishable for the olivine-I and core sections of the groundmass olivine (Fig. 5). Moreover, in many cases the olivine-II cores have their original crystal faces ground away (Figs 7b, h, k, m–q, 8b–e and 9c), and thus their shapes are similar to those of round olivine-I (Figs 2b, 3b and 9a). It is most likely that crystals that now show as relics in the olivine-II cores were formed at depth and transported upwards in a crystal mush.

The chemical resemblance between olivine-I and the cores of olivine-II discovered in this study challenges the existence of different populations of kimberlitic olivine as defined by differences in morphology and size. In other words, our inferred common origin of olivine-I and cores of olivine-II makes it possible to track down the earliest and deepest stages of the kimberlite evolutionary story; that is, when and from where the primary (protokimberlite) magma was derived and started to ascend.

Anatomy of olivine-II: evolutionary storyline of the kimberlite parental melt

The Udachnaya-East groundmass olivine has a clear zoning pattern with the cores having variable Fo values and rims with a limited range in Fo values (Fig. 5b). It should be emphasized again that the olivine-II rims are essentially uniform with respect to major elements, but minor elements fluctuate strongly, especially Ni abundances, which reach maximum values near the core–rim boundary then decrease rapidly towards the outer rims (Figs 5b and 8). Broadly similar compositional features of olivine, with normal and reversed core to rim zonation and similar ranges in Fo and trace element contents, have been previously reported by Mitchell (1986). In more recent literature the same features of groundmass olivine in diamondiferous and barren kimberlites have been emphasized (e.g. Moore, 1988; Skinner, 1989; Fedortchouk & Canil, 2004).

Although the origin of olivine cores (cognate vs exotic) is still debatable, the overall compositional similarity between groundmass olivine from different pipes and different kimberlite provinces argues that: (1) the origin of cores and rims of groundmass olivine is intimately linked to kimberlite genesis and evolution; (2) in each case the physical and chemical conditions of olivine formation are closely similar; (3) olivine cores and rims originate in different conditions; (4) the variable Fo compositions of cores reflect varying sources or changing conditions, whereas the similar Fo values of the olivine rims reflect a major buffering event.

High-pressure origin of olivine-II cores

The presence of relatively common Na- and Cr-enriched high-Ca pyroxene inclusions in the cores of the groundmass olivine (Fig. 9c and d) is indicative of their high-pressure formation. To the best of our knowledge there exists only one report of such Cr-diopside inclusions, in the spheroidal olivine cores from the Igwisi Hills extrusive kimberlites (Reid *et al.*, 1975). Their association with garnet and orthopyroxene inclusions was interpreted in terms of derivation from garnet peridotite at ~1000°C and 50–60 kbar (Reid *et al.*, 1975). Another occurrence of compositionally similar Cr-diopside was recorded as micro-inclusions in diamonds (Stachel & Harris, 1997; Aulbach *et al.*, 2002; Dobosi & Kurat, 2002).

Application of the single-pyroxene geothermobarometer of Nimis & Taylor (2000) to the composition of the high-Ca inclusions provides minimum P–T estimates for the origin of the host olivine-II cores (45–50 kbar and 900–1100°C). These P–T conditions correspond to the diamond stability field in the lower part of lithosphere beneath the Siberian craton (Boyd *et al.*, 1997). Even higher pressures (80–100 kbar) of the kimberlite melt 'take-off' were inferred based on the finding of nanocrystalline (Mg, Fe, Cr)TiO_3 perovskite inclusions in olivine from an ilmenite–garnet–peridotite nodule in the Udachanya-East kimberlite (Wirth & Matsyuk, 2005). Magmatic crystallization of the high-Ca pyroxene inclusions, and by inference their host olivine-II cores, is tentatively supported by the fine-scale compositional zoning of pyroxene crystals and the presence of carbonate–chloride melt inclusions (Fig. 9f). On the other hand, the compositional similarity of high-Ca pyroxene inclusions to diopside in the lherzolite xenoliths of

Udachnaya-East (Fig. 10) indicates a non-magmatic or hybrid origin.

Significant diversity of the groundmass olivine-II cores in shape, size and composition (Figs 7 and 8) suggests different evolutionary paths for individual grains, related to growth, recrystallization, transport, dissolution and regrowth in different mantle–melt and crust–melt environments. The cores with smoothed crystallographic shapes were likely to have precursors as individual phenocrysts that experienced abrasion during upward transport at extremely high speeds, as advocated for the spheroid olivine of the Igwisi kimberlites (Reid *et al.*, 1975). Partial resorption of olivine suggests that primary olivine crystallization became unstable and disequilibrium developed after initial crystallization (Boyd & Clement, 1977; Skinner, 1989), but the causes of this are uncertain. Skinner (1989) proposed crystallization of olivine-II at depth, in small melt pockets before the magma's ascent. However, in such a scenario the viscosity and density of magmas loaded with ~50 vol.% olivine would be high enough to preclude very high speeds of ascent (several hours to several days; Eggler, 1989; Canil & Fedortchouk, 1999; Haggerty, 1999; Kelley & Wartho, 2000; Sparks *et al.*, 2006).

Low-pressure crystallization of olivine-II rims

As noted above, the composition and zoning of the Udachnaya-East olivine-II are not unique; similar principal compositional characteristics of groundmass olivine phenocrysts (variable and constant Fo of cores and rims, respectively, and variable trace elements at a given Fo of the olivine rims; Fig. 5b) have been described in a number of kimberlite suites (e.g. Emeleus & Andrews, 1975; Boyd & Clement, 1977; Mitchell, 1978, 1986; Hunter & Taylor, 1984; Moore, 1988; Kirkley *et al.*, 1989; Skinner, 1989; Fedortchouk & Canil, 2004; Nielsen & Jensen, 2005; Arndt *et al.*, 2006). Compared with the ambiguous origin of the olivine cores (Mitchell, 1986), the rims of olivine-II most certainly crystallized from a melt transporting these crystals to the surface. This is best supported by the cases where several cores of different size, shape and composition are enclosed within a single olivine-II grain (Fig. 7l–q). As indicated by the presence of mineral inclusions, the olivine-II rims (at least some parts of them) formed together with phlogopite, perovskite, minerals of the spinel group, rutile and orthopyroxene (i.e. common groundmass minerals, except orthopyroxene) from a melt similar to that present as melt inclusions in the olivine rims and healed fractures in the olivine-II cores and olivine-I (Figs 4 and 9a). The groundmass olivine crystals are characterized by a tablet shape, which is, according to experimental studies (Donaldson, 1976; Faure *et al.*, 2003), interpreted to be intermediate between the 'steady-state' growth shape (polyhedral crystals) and rapid growth textures (hopper and dendritic crystals), and results from small undercooling (difference between liquidus and growth temperatures).

Numerous studies indicate that most the common mantle xenoliths in kimberlites are garnet lherzolites; however, the surprisingly low abundance of orthopyroxene among xenocrysts and macrocrysts has been puzzling (Mitchell, 1973; Skinner, 1989). Low silica activity in the kimberlite magma has been offered as an explanation for the instability of orthopyroxene, especially at subsurface pressures (Mitchell, 1973). However, the presence of orthopyroxene inclusions in groundmass olivine rims (Fig. 9b) seems to be inconsistent with this hypothesis. One explanation is that orthopyroxene inclusions (often in groups and always associated with CO_2 bubbles; Fig. 9b) can result from the local reaction of olivine with a CO_2 fluid $\left(2SiO_4^{-4} + 2CO_2 \rightarrow Si_2O_6^{-4} + 2CO_3^{-2}\right)$.

The limited range of Fo contents in the olivine-II rims, but variable trace element abundances (Fig. 5b), suggests crystallization over a small temperature range and/or buffering of the magma at a constant Fe^{2+}/Mg (Mitchell, 1986) whilst fractionating Ni, Mn and Ca. In many instances, where the cores are seemingly affected by diffusion (Fig. 7c–f) and have a surrounding layer of distinct composition (Fig. 7f–q), the uniform Fo in the rims could reflect attempts by the crystals to equilibrate with a final hybrid magma (Mitchell, 1986). We also propose that the buffering of Fe^{2+}/Mg can occur if the Mg–Fe distribution coefficient (K_d) between olivine and a carbonate-rich kimberlite melt is significantly higher than that for common basaltic systems (i.e. $0{\cdot}3 \pm 0{\cdot}03$). This reflects the significantly smaller Mg–Fe fractionation between silicates and carbonate melt, possibly as a result of complexing between carbonate and Mg^{2+} ions (Green & Wallace, 1988; Moore, 1988). The implied higher K_d for carbonatitic liquids, and especially Ca-rich carbonate, has been supported by experimental evidence (Dalton & Wood, 1993*a*, 1993*b*; Girnis *et al.*, 2005). We cannot exclude an even more pronounced increase in K_d for alkali-rich carbonatitic liquids.

The melt crystallizing the rims of the Udachnaya-East groundmass olivine is represented by the carbonate–chloride matrix of the rocks (Kamenetsky *et al.*, 2004, 2007*a*, 2007*b*) with an unfractionated chlorine isotope composition (Sharp *et al.*, 2007), and by the melt inclusions in olivine (Figs 4 and 9a; Golovin *et al.*, 2003, 2007; Kamenetsky *et al.*, 2004). The composition of this melt is unusually enriched in alkali carbonates and chlorides, but low in the aluminosilicate component and uniquely low in Al/Si (Kamenetsky *et al.*, 2004, 2007*a*, 2007*b*). The crystallization of olivine from this melt implies saturation in the olivine component, which makes this melt different from the alkali carbonate melt experimentally produced at mantle P–T conditions and low melting

extents (Wallace & Green, 1988; Sweeney *et al.*, 1995). How and where is the saturation in olivine acquired?

Life cycle of kimberlite parental melt

Our study of the olivine populations and complex zoning of the groundmass olivine in the Udachnaya-East kimberlite provides evidence that olivine crystals were first entrapped by the melt at depth, then partly abraded, dissolved and recrystallized on ascent, and finally regenerated during emplacement. We suggest that the history of kimberlitic olivine is owed to the extraordinary melt composition as well as to the conditions during melt generation, transport and emplacement.

In our scenario, a key role is played by the chloride–carbonate (presumably protokimberlite) melt, which probably forms by melting of eclogite (e.g. Gaffney *et al.*, 2007) and thus is undersaturated in olivine and orthopyroxene and has a strong 'garnet' signature. The chloride–carbonate melt is highly buoyant and starts to ascend rapidly, causing mechanical abrasion of the magma pathways in the convecting mantle and lithosphere. Moreover, such a melt is capable of dissolving silicate minerals (e.g. olivine and orthopyroxene) on ascent. The amount of forsterite that can be dissolved in the sodium carbonate liquid at 10 kbar and 1300°C is about 16 wt% (Hammouda & Laporte, 2000), and in our case such contribution is made by dissolution of entrapped olivine $Fo_{85–94}$. Thus this melt accumulates Si and Mg (and to much lesser extent Al from dissolving orthopyroxene), but only to a certain limit, above which an immiscible Cl-bearing carbonate–silicate liquid could appear (Safonov *et al.*, 2007). Ascending kimberlite magma, although being increasingly enriched in the olivine component and loaded with xenocrysts and xenoliths, still remains buoyant and fluid enough to continue fast ascent. On emplacement, the magma releases the dissolved silicate component in the form of groundmass olivine rims (Fo_{89}) and minor silicate minerals (e.g. phlogopite and monticellite), thus driving the residual melt towards the initial (protokimberlite) chloride–carbonate composition (Kamenetsky *et al.*, 2007*a*, 2007*b*). After olivine crystallization the residual chloride–carbonate liquid experiences gravitational separation from other components of the kimberlite magma, such as olivine and other solids (mantle and crustal lithic fragments). Thus the chloride–carbonate melt is squeezed to the top of the kimberlite magma body (e.g. Dawson & Hawthorne, 1973), where combustible gases (e.g. H_2 and CH_4) are released, causing explosion events and formation of the diatreme and crater 'kimberlite' facies. The ultimate fate of the chloride–carbonate melt is both explosive dispersion and rapid degradation in the subsurface environment.

In conclusion, all previous models of kimberlite composition and evolution considered 'uncontaminated' and 'aphanitic' kimberlite rocks as representative of the ultramafic carbonate–silicate kimberlite melt, which is propelled to the surface by exsolution of H_2O and CO_2. On the contrary, we propose that the kimberlite magma originates essentially as a non-silicate, chloride–carbonate liquid that ascends rapidly because of its rheology, acquires ultramafic properties by entraining and dissolving olivine and orthopyroxene *en route* to the surface, and segregates from solids upon emplacement and crystallization.

ACKNOWLEDGEMENTS

This study was inspired by Professor David Green and his insights into nature of low-degree mantle melts, such as carbonatites and kimberlites. The work has greatly benefited from the comments of David Green and Barry Dawson. We are grateful to P. Robinson, S. Gilbert, and K. McGoldrick for assistance with analytical work. We especially thank I. Veksler, G. Yaxley, O. Navon, S. Sparks, I. Ryabchikov, L. Kogarko, D. Canil, F. Costa, Y. Fedortchouk, N. Sobolev, N. Pokhilenko, and D. Ionov for fruitful discussions. The manuscript was substantially improved with a help of insightful reviews by Nick Arndt, Anton le Roex and Greg Yaxley. The work was supported by an Australian Research Council Research and Professorial Fellowships and Discovery Grant to V. Kamenetsky, an Australian Postgraduate Scholarship to M. Kamenetsky, and the A. von Humboldt Foundation (Germany) research funding (Wolfgang Paul Award to A. Sobolev and Friedrich Wilhelm Bessel Award to V. Kamenetsky). S. Demouchy is supported by the LPI postdoctoral fellowship and NSF. A. Golovin acknowledges funding from the Russian Foundation for Basic Research (project 07-05-00072).

SUPPLEMENTARY DATA

Supplementary data for this paper are available at *Journal of Petrology* online.

REFERENCES

Arndt, N. T., Boullier, A. M., Clement, J. P., Dubois, M. & Schissel, D. (2006). What olivine, the neglected mineral, tells us about kimberlite petrogenesis. *eEarth* **1**, 15–21, www.electronic-earth.net/11/15/2006/.

Aulbach, S., Stachel, T., Viljoen, K. S., Brey, G. P. & Harris, J. W. (2002). Eclogitic and websteritic diamond sources beneath the Limpopo Belt—is slab-melting the link? *Contributions to Mineralogy and Petrology* **143**, 56–70.

Barashkov, I. P. & Mahotko, V. F. (1977). About two generations of olivine in the kimberlite rocks (example from Udachnaya-East pipe, Yakutia). In: Kovalskii, V. V. & Oleinikov, B. V. (eds) *Petrology and Geochemistry of Kimberlite Magmas at Early Evolutionary Stages*. Yakutsk: Geological Institute, Academy of Sciences of USSR, pp. 100–107.

Bell, D. R., Rossman, G. R., Maldener, J., Endisch, D. & Rauch, F. (2003). Hydroxide in olivine: a quantitative determination of the absolute amount and calibration of the IR spectrum. *Journal of Geophysical Research* **108**, 2105, doi:2110.1029/2001JB000679.

Boyd, F. R. & Clement, C. R. (1977). Compositional zoning of olivines in kimberlites from the De Beers mine, Kimberley, South Africa. *Carnegie Institution of Washington Yearbook* **76**, 485–493.

Boyd, F. R., Pokhilenko, N. P., Pearson, D. G., Mertzman, S. A., Sobolev, N. V. & Finger, L. W. (1997). Composition of the Siberian cratonic mantle: evidence from Udachnaya peridotite xenoliths. *Contributions to Mineralogy and Petrology* **128**, 228–246.

Brenan, J. M. & Watson, E. B. (1991). Partitioning of trace elements between carbonate melt and clinopyroxene and olivine at mantle *P–T* conditions. *Geochimica et Cosmochimica Acta* **55**, 2203–2214.

Brey, G. & Green, D. H. (1976). The solubility of CO_2 in olivine melilitite at high pressures and the role of CO_2 in the Earth's upper mantle. *Contributions to Mineralogy and Petrology* **55**, 217–230.

Canil, D. & Fedortchouk, Y. (1999). Garnet dissolution and the emplacement of kimberlites. *Earth and Planetary Science Letters* **167**, 227–237.

Dalton, J. A. & Wood, B. J. (1993*a*). The compositions of primary carbonate melts and their evolution through wallrock reaction in the mantle. *Earth and Planetary Science Letters* **119**, 511–525.

Dalton, J. A. & Wood, B. J. (1993*b*). The partitioning of Fe and Mg between olivine and carbonate and the stability of carbonate under mantle conditions. *Contributions to Mineralogy and Petrology* **114**, 501–509.

Dawson, J. B. (1980). *Kimberlites and their Xenoliths*. Berlin: Springer.

Dawson, J. B. (1994). Quaternary kimberlitic volcanism on the Tanzania craton. *Contributions to Mineralogy and Petrology* **116**, 473–485.

Dawson, J. B. & Hawthorne, J. B. (1973). Magmatic sedimentation and carbonatitic differentiation in kimberlite sills at Benfontein, South Africa. *Journal of the Geological Society, London* **129**, 61–85.

Demouchy, S., Jacobsen, S. D., Gaillard, F. & Stern, C. R. (2006). Rapid magma ascent recorded by water diffusion profiles in mantle olivine. *Geology* **34**, 429–432.

Dobosi, G. & Kurat, G. (2002). Trace element abundances in garnets and clinopyroxenes from diamondites—a signature of carbonatitic fluids. *Mineralogy and Petrology* **76**, 21–38.

Donaldson, C. H. (1976). An experimental investigation of olivine morphology. *Contributions to Mineralogy and Petrology* **57**, 187–213.

Edgar, A. D. & Charbonneau, H. E. (1993). Melting experiments on a SiO_2-poor, CaO-rich aphanitic kimberlite from 5–10 GPa and their bearing on sources of kimberlite magmas. *American Mineralogist* **78**, 132–142.

Edgar, A. D., Arima, M., Baldwin, D. K., Bell, D. R., Shee, S. R., Skinner, E. M. W. & Walker, E. C. (1988). High-pressure–high-temperature melting experiments on a SiO_2-poor aphanitic kimberlite from the Wesselton mine, Kimberley, South Africa. *American Mineralogist* **73**, 524–533.

Eggler, D. H. (1989). . In: Ross, J., Jaques, A. L., Ferguson, J., Green, D. H., O'Reilly, S. Y., Danchin, R. V. & Janse, A. J. A. (eds) Kimberlites: how do they form? *Kimberlites and Related Rocks: their Composition, Occurrence, Origin and Emplacement*. Sydney: Blackwell Scientific Publications, pp. 489–504.

Eiler, J. M., Crawford, A., Elliott, T., Farley, K. A., Valley, J. W. & Stolper, E. M. (2000). Oxygen isotope geochemistry of oceanic-arc lavas. *Journal of Petrology* **41**, 229–256.

Emeleus, C. H. & Andrews, J. R. (1975). Mineralogy and petrology of kimberlite dyke and sheet intrusions and included peridotite xenoliths from South West Greenland. *Physics and Chemistry of the Earth* **9**, 179–198.

Falloon, T. J. & Green, D. H. (1989). The solidus of carbonated, fertile peridotite. *Earth and Planetary Science Letters* **94**, 364–370.

Falloon, T. J. & Green, D. H. (1990). Solidus of carbonated fertile peridotite under fluid-saturated conditions. *Geology* **18**, 195–199.

Faure, F., Trolliard, G., Nicollet, C. & Montel, J. M. (2003). A developmental model of olivine morphology as a function of the cooling rate and the degree of undercooling. *Contributions to Mineralogy and Petrology* **145**, 251–263.

Fedortchouk, Y. & Canil, D. (2004). Intensive variables in kimberlite magmas, Lac de Gras, Canada and implications for diamond survival. *Journal of Petrology* **45**, 1725–1745.

Gaffney, A. M., Blichert-Toft, J., Nelson, B. K., Bizzarro, M., Rosing, M. & Albarède, F. (2007). Constraints on source-forming processes of West Greenland kimberlites inferred from Hf–Nd isotope systematics. *Geochimica et Cosmochimica Acta* **71**, 222–238.

Girnis, A. V. & Ryabchikov, I. D. (2005). Conditions and mechanisms of generation of kimberlite magmas. *Geology of Ore Deposits* **47**, 476–487.

Girnis, A. V., Bulatov, V. K. & Brey, G. P. (2005). Transition from kimberlite to carbonatite melt under mantle parameters: an experimental study. *Petrology* **13**, 1–15.

Golovin, A. V., Sharygin, V. V., Pokhilenko, N. P., Mal'kovets, V. G., Kolesov, B. A. & Sobolev, N. V. (2003). Secondary melt inclusions in olivine from unaltered kimberlites of the Udachnaya-East pipe, Yakutia. *Doklady Earth Sciences* **388**, 93–96.

Golovin, A. V., Sharygin, V. V. & Pokhilenko, N. P. (2007). Melt inclusions in olivine phenocrysts in unaltered kimberlites from the Udachnaya-East pipe, Yakutia: some aspects of kimberlite magma evolution during late crystallization stages. *Petrology* **15**, 168–183.

Green, D. H. (1990). The role of oxidation–reduction and C–H–O fluids in determining melting conditions and magma compositions in the upper mantle. *Proceedings of the Indian Academy of Sciences (Earth and Planetary Sciences)* **99**, 153–165.

Green, D. H. & Wallace, M. E. (1988). Mantle metasomatism by ephemeral carbonatite melts. *Nature* **336**, 459–462.

Green, D. H., Taylor, W. R. & Foley, S. (1990). The Earth's upper mantle as a source for volatiles. In: Herbert, H. K. & Ho, S. E. (eds) *Stable Isotopes and Fluid Processes in Mineralization*. Perth: University of Western Australia, pp. 17–34.

Haggerty, S. E. (1999). A diamond trilogy: superplumes, supercontinents, and supernovae. *Science* **285**, 851–860.

Hammouda, T. & Laporte, D. (2000). Ultrafast mantle impregnation by carbonatite melts. *Geology* **28**, 283–285.

Hunter, R. H. & Taylor, L. A. (1984). Magma-mixing in the low velocity zone: kimberlitic megacrysts from Fayette County, Pennsylvania. *American Mineralogist* **69**, 16–29.

Kamenetsky, M. B., Sobolev, A. V., Kamenetsky, V. S., Maas, R., Danyushevsky, L. V., Thomas, R., Sobolev, N. V. & Pokhilenko, N. P. (2004). Kimberlite melts rich in alkali chlorides and carbonates: a potent metasomatic agent in the mantle. *Geology* **32**, 845–848.

Kamenetsky, V. S., Kamenetsky, M. B., Sharygin, V. V., Faure, K. & Golovin, A. V. (2007*a*). Chloride and carbonate immiscible liquids at the closure of the kimberlite magma evolution (Udachnaya-East kimberlite, Siberia). *Chemical Geology* **237**, 384–400.

Kamenetsky, V. S., Kamenetsky, M. B., Sharygin, V. V. & Golovin, A. V. (2007*b*). Carbonate–chloride enrichment in fresh kimberlites of the Udachnaya-East pipe, Siberia: a clue to physical properties of kimberlite magmas?. *Geophysical Research Letters* **34**, L09316, doi:09310.01029/02007GL029389.

Kelley, S. P. & Wartho, J. A. (2000). Rapid kimberlite ascent and the significance of Ar–Ar ages in xenolith phlogopites. *Science* **289**, 609–611.

Kirkley, M. B., Smith, H. S. & Gurney, J. J. (1989). Kimberlite carbonates—a carbon and oxygen stable isotope study. In: Ross, J., Jaques, A. L., Ferguson, J., Green, D. H., O'Reilly, S. Y., Danchin, R. V. & Janse, A. J. A. (eds) *Kimberlites and Related Rocks: their Composition, Occurrence, Origin and Emplacement*. Sydney: Blackwell Scientific Publications, pp. 264–281.

le Roex, A. P., Bell, D. R. & Davis, P. (2003). Petrogenesis of group I kimberlites from Kimberley, South Africa: evidence from bulk-rock geochemistry. *Journal of Petrology* **44**, 2261–2286.

Libowitzky, E. & Rossman, G. R. (1996). Principles of quantitative absorbance measurements in anisotropic crystals. *Physics and Chemistry of Minerals* **23**, 319–327.

Maas, R., Kamenetsky, M. B., Sobolev, A. V., Kamenetsky, V. S. & Sobolev, N. V. (2005). Sr, Nd, and Pb isotope evidence for a mantle origin of alkali chlorides and carbonates in the Udachnaya kimberlite, Siberia. *Geology* **33**, 549–552.

Marshintsev, V. K. (1986). *Vertical Heterogeneity of Kimberlite Bodies in Yakutiya*. Novosibirsk: Nauka.

Marshintsev, V. K., Migalkin, K. N., Nikolaev, N. C. & Barashkov, Y. P. (1976). Unaltered kimberlite of the Udachnaya East pipe. *Transactions (Doklady) of the USSR Academy of Sciences* **231**, 961–964.

Matsyuk, S. S. & Langer, K. (2004). Hydroxyl in olivines from mantle xenoliths in kimberlites of the Siberian platform. *Contributions to Mineralogy and Petrology* **147**, 413–437.

Mattey, D., Lowry, D. & Macpherson, C. (1994). Oxygen-isotope composition of mantle peridotite. *Earth and Planetary Science Letters* **128**, 231–241.

Miller, G. H., Rossman, G. R. & Harlow, G. E. (1987). The natural occurrence of hydroxide in olivine. *Physics and Chemistry of Minerals* **14**, 461–472.

Mitchell, R. H. (1973). Composition of olivine, silica activity and oxygen fugacity in kimberlite. *Lithos* **6**, 65–81.

Mitchell, R. H. (1978). Mineralogy of the Elwin Bay kimberlite, Somerset Island, N.W.T., Canada. *American Mineralogist* **63**, 47–57.

Mitchell, R. H. (1986). *Kimberlites: Mineralogy, Geochemistry and Petrology*. New York: Plenum.

Mitchell, R. H. (1989). Aspects of the petrology of kimberlites and lamproites: some definitions and distinctions. In: Ross, J., Jaques, A. L., Ferguson, J., Green, D. H., O'Reilly, S. Y., Danchin, R. V. & Janse, A. J. A. (eds) *Kimberlites and Related Rocks: their Composition, Occurrence, Origin and Emplacement*. Sydney: Blackwell Scientific Publications, pp. 7–45.

Mitchell, R. H. (1995). *Kimberlites, Orangeites and Related Rocks*. New York: Plenum.

Moore, A. E. (1988). Olivine: a monitor of magma evolutionary paths in kimberlites and olivine melilitites. *Contributions to Mineralogy and Petrology* **99**, 238–248.

Nielsen, T. F. D. & Jensen, S. M. (2005). The Majuagaa calcite-kimberlite dyke, Maniitsoq, southern West Greenland. *Geological Survey of Denmark and Greenland, Report* 2005/43, 59.

Nimis, P. & Taylor, W. R. (2000). Single clinopyroxene thermobarometry for garnet peridotites. Part I. Calibration and testing of a Cr-in-Cpx barometer and an enstatite-in-Cpx thermometer. *Contributions to Mineralogy and Petrology* **139**, 541–554.

Pasteris, J. D. (1984). Kimberlites: complex mantle melts. *Annual Review of Earth and Planetary Sciences* **12**, 133–153.

Paterson, M. S. (1982). The determination of hydroxyl by infrared absorption in quartz, silicate glasses and similar materials. *Bulletin de Minéralogie* **105**, 20–29.

Pearson, D. G., Shirey, S. B., Carlson, R. W., Boyd, F. R., Pokhilenko, N. P. & Shimizu, N. (1995). Re–Os, Sm–Nd, and Rb–Sr isotope evidence for thick Archaean lithospheric mantle beneath the Siberian craton modified by multistage metasomatism. *Geochimica et Cosmochimica Acta* **59**, 959–977.

Perkins, G. B., Sharp, Z. D. & Selverstone, J. (2006). Oxygen isotope evidence for subduction and rift-related mantle metasomatism beneath the Colorado Plateau–Rio Grande rift transition. *Contributions to Mineralogy and Petrology* **151**, 633–650.

Peslier, A. H. & Luhr, J. F. (2006). Hydrogen loss from olivines in mantle xenoliths from Simcoe (USA) and Mexico: mafic alkalic magma ascent rates and water budget of the sub-continental lithosphere. *Earth and Planetary Science Letters* **242**, 302–319.

Price, S. E., Russell, J. K. & Kopylova, M. G. (2000). Primitive magma from the Jericho Pipe, NWT, Canada: constraints on primary kimberlite melt chemistry. *Journal of Petrology* **41**, 789–808.

Reid, A. M., Donaldson, C. H., Dawson, J. B., Brown, R. W. & Ridley, W. I. (1975). The Igwisi Hills extrusive 'kimberlites'. *Physics and Chemistry of the Earth* **9**, 199–218.

Safonov, O. G., Perchuk, L. L. & Litvin, Y. A. (2007). Melting relations in the chloride–carbonate–silicate systems at high-pressure and the model for formation of alkalic diamond-forming liquids in the upper mantle. *Earth and Planetary Science Letters* **253**, 112–128.

Sharp, Z. D. (1990). A laser-based microanalytical method for the *in situ* determination of oxygen isotope ratios of silicates and oxides. *Geochimica et Cosmochimica Acta* **54**, 1353–1357.

Sharp, Z. D., Barnes, J. D., Brearley, A. J., Fischer, T., Chaussidon, M. & Kamenetsky, V. S. (2007). Chlorine isotope homogeneity of the mantle, crust and carbonaceous chondrites. *Nature* **446**, 1062–1065.

Sharygin, V. V., Golovin, A. V., Pokhilenko, N. P. & Kamenetsky, V. S. (2007). Djerfisherite in the Udachnaya-East pipe kimberlites (Sakha–Yakutia, Russia): paragenesis, composition and origin. *European Journal of Mineralogy* **19**, 51–63.

Shee, S. R. (1986). The petrogenesis of the Wesselton mine kimberlites, Kimberley, South Africa. Ph.D. thesis, University of Cape Town.

Shimizu, N., Pokhilenko, N. P., Boyd, F. R. & Pearson, D. G. (1997). Geochemical characteristics of mantle xenoliths from Udachnaya kimberlite pipe. *Russian Geology and Geophysics* **38**, 194–205.

Skinner, E. M. W. (1989). Contrasting Group I and Group II kimberlite petrology: towards a genetic model for kimberlites. In: Ross, J., Jaques, A. L., Ferguson, J., Green, D. H., O'Reilly, S. Y., Danchin, R. V. & Janse, A. J. A. (eds) *Kimberlites and Related Rocks: their Composition, Occurrence, Origin and Emplacement*. Sydney: Blackwell Scientific Publications, pp. 528–544.

Smith, C. B. (1983). Pb, Sr and Nd isotopic evidence for sources of southern African Cretaceous kimberlites. *Nature* **304**, 51–54.

Sobolev, N. V. (1977). In: Boyd, F. R. (ed.) *Deep-seated Inclusions in Kimberlites and the Problem of the Composition of the Upper Mantle*. Washington, DC: American Geophysical Union, 279 p.

Sobolev, A. V., Sobolev, N. V., Smith, C. B. & Dubessy, J. (1989). Fluid and melt compositions in lamproites and kimberlites based on the study of inclusions in olivine. In: Ross, J., Jaques, A. L., Ferguson, J., Green, D. H., O'Reilly, S. Y., Danchin, R. V. & Janse, A. J. A. (eds) *Kimberlites and Related Rocks: their Composition, Occurrence, Origin and Emplacement*. Sydney: Blackwell Scientific Publications, pp. 220–241.

Sobolev, A. V., Hofmann, A. W., Kuzmin, D. V., Yaxley, G. M., Arndt, N. T., Chung, S.-L., Danyushevsky, L. V., Elliott, T., Frey, F. A., Garcia, M. O., Gurenko, A. A., Kamenetsky, V. S., Kerr, A. C., Krivolutskaya, N. A., Matvienkov, V. V., Nikogosian, I. K., Rocholl, A., Sigurdsson, I. A., Sushchevskaya, N. M. & Teklay, M. (2007). The amount of recycled crust in sources of mantle-derived melts. *Science* **316**, 412–417.

Sparks, R. S. J., Baker, L., Brown, R. L., Field, M., Schumacher, J., Stripp, G. & Walters, A. (2006). Dynamical constraints on kimberlite volcanism. *Journal of Volcanology and Geothermal Research* **155**, 18–48.

Stachel, T. & Harris, J. W. (1997). Diamond precipitation and mantle metasomatism—evidence from the trace element chemistry of silicate inclusions in diamonds from Akwatia, Ghana. *Contributions to Mineralogy and Petrology* **129**, 143–154.

Sun, S.-S. & McDonough, W. F. (1989). Chemical and isotopic systematics of oceanic basalts: implications for mantle composition and processes. In: Saunders, A. D. & Norry, M. J. (eds) *Magmatism in the Ocean Basins. Geological Society, London, Special Publications* **42**, 313–345.

Sweeney, R. J., Falloon, T. J. & Green, D. H. (1995). Experimental constraints on the possible mantle origin of natrocarbonatite. In: Bell, K. & Keller, J. (eds) *Carbonatite Volcanism: Oldoinyo Lengai and Petrogenesis of Natrocarbonatites*. Berlin: Springer, pp. 191–207.

Wallace, M. E. & Green, D. H. (1988). An experimental determination of primary carbonatite magma composition. *Nature* **335**, 343–346.

Watkinson, D. H. & Chao, G. Y. (1973). Shortite in kimberlite from the Upper Canada Gold Mine, Ontario. *Journal of Geology* **81**, 229–233.

Wirth, R. & Matsyuk, S. (2005). Nanocrystalline (Mg, Fe, Cr)TiO_3 perovskite inclusions in olivine from a mantle xenolith, Udachnaya-East kimberlite pipe, Siberia. *Earth and Planetary Science Letters* **233**, 325–336.

Yaxley, G. M. & Green, D. H. (1996). Experimental reconstruction of sodic dolomitic carbonatite melts from metasomatised lithosphere. *Contributions to Mineralogy and Petrology* **124**, 359–369.

Yaxley, G. M., Crawford, A. J. & Green, D. H. (1991). Evidence for carbonatite metasomatism in spinel peridotite xenoliths from western Victoria, Australia. *Earth and Planetary Science Letters* **107**, 305–317.

Yaxley, G. M., Green, D. H. & Kamenetsky, V. (1998). Carbonatite metasomatism in the southeastern Australian lithosphere. *Journal of Petrology* **39**, 1917–1930.

Zinchuk, N. N., Spetsius, Z. V., Zuenko, V. V. & Zuev, V. M. (1993). *Udachnaya kimberlite pipe*. Novosibirsk: University of Novosibirsk.